NIH Public Access
Author Manuscript
Exp Eye Res. Author manuscript; available in PMC 2016 January 01.

Published in final edited form as:
Exp Eye Res. 2015 January ; 130: 17–28. doi:10.1016/j.exer.2014.11.010.

The rat retina has five types of ganglion-cell photoreceptors

Aaron N. Reifler[1], **Andrew P. Chervenak**[1], **Michael E. Dolikian**[1], **Brian A. Benenati**, **Benjamin S. Meyers**, **Zachary D. Demertzis**, **Andrew M. Lynch**, **Benjamin Y. Li**, **Rebecca D. Wachter**, **Fady S. Abufarha**, **Eden A. Dulka**, **Weston Pack**, **Xiwu Zhao**, and **Kwoon Y. Wong**[2]
Department of Ophthalmology & Visual Sciences, and Department of Molecular, Cellular & Developmental Biology, University of Michigan, Ann Arbor, MI 48105

Abstract

Intrinsically photosensitive retinal ganglion cells (ipRGCs) are inner retinal photoreceptors that mediate non-image-forming visual functions, e.g. pupillary constriction, regulation of pineal melatonin release, and circadian photoentrainment. Five types of ipRGCs were recently discovered in mouse, but whether they exist in other mammals remained unknown. We report that the rat also has five types of ipRGCs, whose morphologies match those of mouse ipRGCs; this is the first demonstration of all five cell types in a non-mouse species. Through immunostaining and λ_{max} measurements, we showed that melanopsin is likely the photopigment of all rat ipRGCs. The various cell types exhibited diverse spontaneous spike rates, with the M1 type spiking the least and M4 spiking the most, just like we had observed for their mouse counterparts. Also similar to mouse, all ipRGCs in rat generated not only sluggish intrinsic photoresponses but also fast, synaptically driven ones. However, we noticed two significant differences between these species. First, whereas we learned previously that all mouse ipRGCs had equally sustained synaptic light responses, rat M1 cells' synaptic photoresponses were far more transient than those of M2–M5. Since M1 cells provide all input to the circadian clock, this rat-versus-mouse discrepancy could explain the difference in photoentrainment threshold between mouse and other species. Second, rat ipRGCs' melanopsin-based spiking photoresponses could be classified into three varieties, but only two were discerned for mouse ipRGCs. This correlation of spiking photoresponses with cell types will help researchers classify ipRGCs in multielectrode-array (MEA) spike recordings.

Keywords

Melanopsin; intrinsically photosensitive retinal ganglion cell; ipRGC; light response; whole-cell recording; photoreceptors; circadian photoentrainment; synaptic transmission

© 2014 Elsevier Ltd. All rights reserved.

[2]Corresponding author: 1000 Wall Street, Ann Arbor, MI 48105. kwoon@umich.edu. Telephone: 734-936-5068.
[1]Equal contributions.

Publisher's Disclaimer: This is a PDF file of an unedited manuscript that has been accepted for publication. As a service to our customers we are providing this early version of the manuscript. The manuscript will undergo copyediting, typesetting, and review of the resulting proof before it is published in its final citable form. Please note that during the production process errors may be discovered which could affect the content, and all legal disclaimers that apply to the journal pertain.

NIH-PA Author Manuscript
NIH-PA Author Manuscript
NIH-PA Author Manuscript

NIH-PA Author Manuscript
NIH-PA Author Manuscript
NIH-PA Author Manuscript

1. Introduction

Intrinsically photosensitive retinal ganglion cells (ipRGCs) are mammalian retinal output neurons that contain the photopigment melanopsin (Provencio et al., 1998) and function as photoreceptors. They mediate non-image-forming photoresponses such as pupil reflexes, entrainment of circadian rhythms to light/dark cycles, and regulation of pineal melatonin secretion. IpRGCs were discovered by David Berson and colleagues (Berson et al., 2002) who labeled them in rats through retrograde transport of dyes injected into the suprachiasmatic nucleus (SCN), site of the circadian clock. All retrolabeled ipRGCs shared a common morphology, suggesting they constitute a single cell type. Specifically, their somas were intermediate in size among neurons in the ganglion cell layer (GCL), and their long, tortuous dendrites branched sparsely and terminated in the OFF sublamina of the inner plexiform layer (IPL) (Berson et al., 2002). Another study of SCN-projecting rat ipRGCs also described them as having sparse and tortuous dendrites, though three dendritic stratification patterns were seen: ON, OFF, and ON/OFF (Warren et al., 2003). However, all cells' dendrites appeared to project toward the OFF sublamina, suggesting they ultimately terminated in that sublamina just like those described by Berson *et al*.

Subsequent studies revealed five morphological types of ipRGCs in mouse. The SCN-projecting type, with morphology virtually identical to that in rat, is named M1, whereas the new types are called M2 through M5 (Ecker et al., 2010; Viney et al., 2007). M2 cells have sparse, irregular dendrites confined to the ON sublamina of the IPL. M3 cells have both ON- and OFF-terminating dendrites. M4 cells have large somas and dense, radiate dendrites restricted to the ON sublamina, and seem identical to the previously described ON alpha cells (Estevez et al., 2012; Schmidt et al., 2014). M5's dendrites are also restricted to the ON sublamina, but they have a bushy appearance and cover a relatively narrow field (Ecker et al., 2010; Hu et al., 2013).

It is unknown whether other mammalian species also possess these five ipRGC types. Besides mouse, ipRGCs have been investigated most extensively in rat. Early rat studies observed melanopsin antibody staining only in the OFF sublamina, consistent with the existence of just the M1 type (Boudard et al., 2009; Hattar et al., 2002; Li et al., 2006; Ostergaard et al., 2007; Warren et al., 2006). Multielectrode-array (MEA) recordings of rat ipRGCs likewise failed to show obvious photoresponse heterogeneity (Weng et al., 2009). More recently, researchers began to notice melanopsin-immunopositive dendrites in the ON sublamina (Engelund et al., 2010; Hannibal et al., 2013; Ingham et al., 2009). By tracing the dendrites of individual melanopsin-immunopositive rat RGCs, a recent study detected M2 and M3 cells in addition to M1 cells (Esquiva et al., 2013). Pilot studies on rat retinas have also revealed rod/cone-independent light responses in M4-like ON alpha cells (Estevez et al., 2012). But M5 has not been found in rat, and M1 and M4 remain the only ipRGC types to have been unequivocally recorded in this species.

Here, we report that the rat has all five morphological types of ipRGCs. We further show that they are physiologically diverse, differing in spontaneous and light-evoked electrical activities. Finally, we compare and contrast their light-driven spiking responses with those of mouse ipRGCs.

NIH-PA Author Manuscript

NIH-PA Author Manuscript

NIH-PA Author Manuscript

2. Material and methods

Animals and eyecup preparation

All procedures were approved by the University Committee on Use and Care of Animals at the University of Michigan. Sprague Dawley rats of both genders were used, and ages ranged from 7 weeks to 4 months. Animals were housed in a 12hr-light/12hr-dark cycle, with all experiments conducted during the light phase.

Prior to each experiment, a rat was dark-adapted in a ventilated light-proof box overnight. Under dim red light, the animal was euthanized using carbon dioxide, then secondary euthanasia by bilateral pneumothorax or cervical dislocation. Both eyes were harvested and hemisected. After removal of the vitreous using forceps, the eyecups were transferred to room-temperature Ames' medium gassed with 95% O_2 5% CO_2. Each eyecup was cut into quadrants, which were kept in darkness for up to 9 hr before being used for whole-cell recording.

Whole-cell recording, light stimulation, and chemicals

An eyecup quadrant was flattened with the scleral side down on the transparent bottom of a custom-made superfusion chamber and held down by a weighted net. The chamber was mounted on a fixed-stage upright microscope (Eclipse FN1; Nikon Instruments, Melville, NY). The bathing solution was Ames' medium gassed with 95% O_2 5% CO_2, which was maintained at 32 °C using a temperature controller (Warner Instruments, Hamden, CT) and fed into the superfusion chamber by a peristaltic pump at 2 – 3 mL/min. The preparation was kept in darkness except during stimulus light presentation.

The GCL was visualized through infrared transillumination and whole-cell current-clamp recording obtained from randomly selected somas using either a MultiClamp 700A or 700B amplifier (Molecular Devices; Sunnyvale, CA). Glass micropipettes with tip resistances 6 – 10 MΩ were pulled from thick-walled borosilicate tubings on a Narishige PC-10 puller (East Meadow, NY), and were filled with an intracellular solution containing (in mM): 120 K-gluconate; either 9 Neurobiotin-Cl (Vector Laboratories; Burlingame, CA) or 5 NaCl plus 4 KCl; 10 Hepes; 2 EGTA; 4 Mg-ATP; 0.3 Na-GTP; 7 Tris-phosphocreatine; 0.1% Lucifer Yellow; and KOH to set pH at 7.3. Using Molecular Devices CLAMPEX software, the liquid junction potential was calculated to be ~13 mV, which was taken into account in all recordings. PCLAMP 9 or 10 software (Molecular Devices) was used to acquire data. Signals were low-pass filtered at 2.4 kHz and sampled at 5 kHz. Series resistances ranged from 15 to 40 MΩ and were not compensated.

Stimuli were uniform full-field lights presented from below the superfusion chamber's transparent bottom, with intensity and wavelength adjusted using neutral density (ND) and narrowband filters respectively. Unless stated otherwise, stimulus wavelength was 480 nm. A PCLAMP-driven electromechanical shutter regulated stimulus timing. Because the experiments were performed on two rigs over >3 years using several sets of filters, stimulus intensities varied somewhat between the rigs and over time. When averaging photoresponses (Figs. 3, 4, and 5A–C), we pooled all the responses to stimuli produced using the same neutral density factor (e.g. ND2), and expressed light intensity as the midpoint of the

NIH-PA Author Manuscript

NIH-PA Author Manuscript

NIH-PA Author Manuscript

intensity range ± half of that range. For example, "14.6±0.1 log photons cm^{-2} s^{-1}" denotes 14.5 log photons cm^{-2} s^{-1} to 14.7 log photons cm^{-2} s^{-1}. Light intensities were measured using a UDT S370 radiometer (Gamma Scientific, San Diego, CA) with a rat eyecup covering the photodiode.

In the experiments examining melanopsin-based light responses, rod/cone signaling was blocked by 50 μM L(+)-2-amino-4-phosphonobutyrate (L-AP4, an agonist for group III metabotropic glutamate receptors), 40 μM 6,7-dinitroquinoxaline2,3-dione (DNQX, an AMPA/kainate receptor antagonist), and 25 μM D-2-amino-5-phosphonovalerate (D-AP5, an NMDA receptor antagonist). These glutamate analogs were purchased from Tocris (Minneapolis, MN). Unless stated otherwise, all other chemicals were purchased from Sigma (St Louis, MO).

Data analysis

The analyses shown in Figs. 3C and 4C–E were based on graded photoresponses, and measurements were made after the recordings had been low-pass filtered at 10 Hz. Photoresponse amplitude was measured relative to the pre-stimulus baseline. The latency to peak of a light response was measured relative to stimulus onset. In the experiment estimating the λ_{max} of intrinsic photoresponses, we assumed these responses were mediated by an opsin-based photopigment. Two to four sub-saturating intensities of 480-nm and 580-nm light steps with 10-sec duration were presented to each cell during rod/cone signaling block. Peak amplitudes of the responses were plotted versus stimulus intensities (Fig. 4E), and the lateral displacement between the 480-nm and 580-nm curves was measured at about 1/3 to half the maximal value of the 480-nm curve, where the two curves tended to be most parallel. Using the nomogram describing the spectral shape shared by all mammalian opsin-based photopigments (Lamb, 1995), the λ_{max} value for which the sensitivity difference between 480 nm and 580 nm matches this lateral displacement was identified.

For the analyses shown in Fig. 5, CLAMPFIT software (Molecular Devices) was used to detect spikes and measure spike timing. The spikes of some cells (especially M1 cells) exhibited significant depolarization block during a light response (Figs. 3A and 4A); all "spikelets" under 2 mV in amplitude were excluded from these analyses. Each photoresponse was represented by a spike histogram with 1-sec bin width. For cells that spiked spontaneously in darkness, the baseline of each spike histogram was "zeroed" by subtracting the mean pre-stimulus spike rate from the entire histogram. The height of the tallest column in the baseline-zeroed histogram was used as the peak response amplitude. The timing of this tallest column relative to stimulus onset corresponded to the latency of peak of the response.

All statistical comparisons were made using the unpaired Student's *t* test, with the significance level set at a *p*-value of 0.05. All error values and error bars represent S.E.M. unless stated otherwise. In the figures and table, *p*-values are represented by asterisks: *, $p < 0.05$; **, $p < 0.01$; ***, $p < 0.001$.

NIH-PA Author Manuscript

NIH-PA Author Manuscript

NIH-PA Author Manuscript

Immunohistochemistry and morphological analysis

Immediately after recording from a cell exhibiting intrinsic light responses, the cell's Lucifer Yellow fill was imaged using epifluorescence. The retina was isolated from the sclera, fixed in phosphate buffer saline (PBS) containing 4% paraformaldehyde for 12 – 20 min, washed 4 times in PBS, incubated for 2 hr in the primary block solution (10% donkey serum and 0.5% Triton X-100 in PBS), and stored at 4 °C for 5 days in primary block solution containing goat-anti-choline acetyltransferase (ChAT) antibody (EMD Millipore AB144P, 1:200; Billerica, MA) and either Alexa488-conjugated streptavidin (1:800; Life Technologies; Grand Island, NY) for Neurobiotin-filled cells or rabbit-anti-Lucifer Yellow antibody (Life Technologies A5750, 1:500) for cells without Neurobiotin. For some Neurobiotin-filled cells, this 5-day primary incubation also included rabbit-anti-melanopsin antibody (Thermo Fisher Scientific PA1-780, 1:1000; Waltham MA) or rabbit-anti-RNA-binding protein with multiple splicing (RBPMS) antibody (PhosphoSolutions 1830-RBPMS, 1:300). After 4 rinses in PBS, the retina was transferred to PBS containing 5% donkey serum, 0.25% Triton X-100, donkey-anti-goat Cy3 or Cy5 antibody (1:250; Jackson ImmunoResearch; West Grove, PA), and, if a rabbit primary antibody had been used, donkey-anti-rabbit FITC or Cy3 antibody (1:250; Jackson ImmunoResearch). After 4 rinses in PBS, the retina was mounted on a glass slide with Vectashield (Vector Laboratories), and the recorded cell was imaged at 0.38-μm steps using the 488 nm, 561 nm and 633 nm lasers of a confocal microscope (Leica SP5; Buffalo Grove, IL). Image quality was enhanced through 3D deconvolution (Leica).

Cell types were assigned according to morphological criteria (Ecker et al., 2010; Estevez et al., 2012; Viney et al., 2007). M1, M3 and M5 cells were the easiest to identify because M1 is the only type stratifying exclusively in the OFF sublamina, M3 is the sole bistratifying type, and M5 has uniquely small and bushy dendritic fields. In contrast, it was less straightforward to discriminate M2 from M4 because both have relatively wide dendritic fields stratifying in the ON sublamina. We could readily identify the majority of M4 cells by their very large somas and dense, radially symmetric dendrites, and most M2 cells by their smaller somas and sparse, irregular dendrites. A few ambiguous cases remained, however, because M2 and M4 overlap somewhat in soma size and dendritic density, and because some M2 cells' dendrites may appear somewhat radiate (Estevez et al., 2012). Fortunately, these two ipRGC types differ in one additional way: M2 dendrites almost always stratify more proximally (i.e. more vitreally) than M4 dendrites, so that the latter are closer to the ON ChAT band (Estevez et al., 2012). This stratification difference enabled identification of the ambiguous cells.

Total dendritic length, dendritic-field size and soma size were measured with the help of ImageJ software (National Institutes of Health; Bethesda, MD) and the NeuronJ plugin (http://www.imagescience.org/meijering/software/neuronj). To measure total dendritic length, the z-stack confocal sections of each cell were projected onto a 2-D image and the dendrites traced manually within ImageJ. We measured dendritic-field size by connecting all dendritic tips in each 2-D image with straight lines and calculating the area of the resultant polygon. To measure soma size, we identified the confocal section where the soma was best focused, traced the outline of the soma and calculated the enclosed area. Both dendritic-field

NIH-PA Author Manuscript

NIH-PA Author Manuscript

NIH-PA Author Manuscript

and soma sizes were expressed as the diameter of a circle of equal area. Sholl analysis (Sholl, 1953) was performed using the ImageJ Sholl Analysis Plugin (Anirvan Ghosh, University of California San Diego).

Analysis of data previously collected from mouse ipRGCs

The plots shown in Fig. 5D–F are based on mouse ipRGC recordings from an earlier study (Zhao et al., 2014). Briefly, retinas were isolated from dark-adapted mice whose ipRGCs were selectively labeled with green fluorescent protein (GFP). Retinas were superfused by 32 °C Ames' medium containing 50 μM L-AP4, 40 μM DNQX and 25 μM D-AP5 to block rod/cone signaling, and GFP labeling was visualized using an invisible two-photon laser. Whole-cell current-clamp recordings were made using an intracellular solution containing (in mM): 120 K-gluconate; 5 NaCl; 4 KCl; 10 Hepes; 2 EGTA; 4 Mg-ATP; 0.3 Na-GTP; 7 Tris-phosphocreatine; 0.1% Lucifer Yellow or 0.001% Alexa Fluor568 hydrazide (Life Technologies); and KOH to set pH at 7.3. Cell type was determined based on morphological criteria (Zhao et al., 2014). The stimuli were full-field white lights and intensities are expressed as equivalent 515-nm photon fluxes. Spikes were analyzed as described above for rat ipRGCs.

3. Results

Overview

To search for ipRGCs, we recorded from ~3,200 neurons in the GCL of rat eyecups, randomly sampling from somas of all sizes. Since rat ipRGCs are known to generate sustained depolarizing responses to prolonged light (Berson et al., 2002; Graham et al., 2008; Perez-Leon et al., 2006; Sodhi and Hartwick, 2014; Van Hook and Berson, 2010; Van Hook et al., 2012; Warren et al., 2003, 2006; Weng et al., 2009; Wong, 2012; Wong et al., 2005; Wong et al., 2007a), we presented each cell with 10-sec light steps with intensities from 9.4 log to 14.7 log photons cm^{-2} s^{-1} and looked for those that depolarized throughout at least one of the stimuli. Once a sustained depolarizing cell was found, rod/cone signaling blockers (see Methods) were applied and 10-sec light steps presented again to probe for rod/cone-independent photosensitivity. In the presence of these drugs, 186 cells exhibited sluggish, sustained depolarizing light responses resembling the melanopsin-based photoresponses of ipRGCs (Berson et al., 2002). Seventy-eight of these were identifiable as ganglion cells because they extended an axon toward the retinal surface. For 9 of these axon-bearing cells, immunoreactivity for the retinal ganglion cell (RGC) marker RBPMS (Rodriguez et al., 2014) was assessed and all were stained, confirming they were RGCs. The remaining 108 sustained depolarizing cells had amacrine-like morphologies and were excluded from the present study.

Morphological characterization

As mentioned in the Introduction, the five known types of mouse ipRGCs have different dendritic morphologies, stratification patterns, and soma sizes. Each of the 78 rat ipRGCs we encountered resembled one of the mouse ipRGC types, and will be named M1 – M5. Examples are shown in Fig. 1A. Their differences in soma diameter, dendritic-field diameter, total dendritic length, total branch points and number of primary dendrites are

NIH-PA Author Manuscript

NIH-PA Author Manuscript

NIH-PA Author Manuscript

quantified in Fig. 1B,C and Table 1. For four of these parameters, at least one ipRGC type stood out as being significantly different from all the other types: the largest dendritic field and fewest primary dendrites for M1, the largest soma for M4, and the smallest dendritic field and most branch points for M5 (Table 1B). Remarkably, there was no overlap at all between the soma diameters of M4 and M1 or M3 (Fig. 1B), between the dendritic field diameters of M1 and M5, or between the total branch points of M5 and M1 or M2 (Fig. 1C).

To further characterize dendritic distribution, we performed Sholl analysis, counting the number of dendrites at different distances from the soma center. Though Sholl analysis had previously been performed for rat M1 cells (Li et al., 2006), it had not been done on M2 – M5 of this species. M1 dendrites showed the lowest peak value of ~10, whereas M4 dendrites had the highest peak of ~26. Although M5's peak value of ~24 was nearly as high as M4's, it dropped rapidly with distance and reached zero at ~250 μm from the soma center (Fig. 1B). At this distance, all the other cells still had at least ~3 dendrites on average, confirming that M5's dendritic fields are the smallest among rat ipRGCs.

Melanopsin expression

Melanopsin immunostaining was tested on 17 ipRGCs (4 M1, 6 M2, 1 M3, 4 M4 and 2 M5). Staining was observed in all M1 cells and 2 M2 cells (data not shown), but the remaining cells lacked obvious staining. This result suggests that most non-M1 ipRGCs in rat either do not use melanopsin as their photopigment, or use it with expression levels beneath detection threshold by our antibody staining method. Electrophysiological evidence for the latter possibility will be presented below.

Resting electrophysiological behavior

We previously learned that the five ipRGC types in mouse have different resting membrane potentials and spontaneous spike rates (Zhao et al., 2014). We sought to determine whether rat ipRGCs are similarly diverse in these properties. Example recordings of rat ipRGCs in darkness are shown in Fig. 2A. The mean resting potentials of the five cell types ranged from −63.8±3.4 mV for M3 to −59.2±1.8 mV for M2, although no statistically significant difference was observed between any two types (Fig. 2B). On the other hand, mean spontaneous spike rates spanned a much greater range, from 0.5±0.2 Hz for M1 to 33.2±2.8 Hz for M4. Seven of the ten possible pairwise comparisons were significantly different, especially for M4 *vs.* M1, M4 *vs.* M2, and M4 *vs.* M5 (p-values < 0.001; Fig. 2C). Whereas nearly all non-M1 cells spiked in darkness, half of the M1 cells did not show any spontaneous spiking and the other half did so at no more than 2 Hz.

Light-evoked responses

The remaining experiments compared the various ipRGC types' light responses. The first experiment was done during superfusion by normal Ames' medium to permit extrinsic, synaptically driven responses as well as intrinsic responses. Fig. 3A shows example responses to 10-sec light steps of three intensities, and Fig. 3B shows averaged responses with all spikes removed through 10 Hz low-pass filtering so that the response waveforms can be seen unobstructed.

NIH-PA Author Manuscript

NIH-PA Author Manuscript

NIH-PA Author Manuscript

The lowest intensity, 9.5±0.1 log photons cm^{-2} s^{-1}, evoked purely rod/cone-driven responses because it was below all ipRGCs' intrinsic photoresponse thresholds (Figs. 4B,D, and 5A,C) (Wong, 2012). While all cell types' responses were depolarizing, their kinetics differed: they were small and lasted only 1 – 2 sec for M1, but more robust and sustained for M2 – M5 (Figs. 3A and 3B). To quantify these kinetics differences, we measured each cell's response amplitude at the peak and just before cessation of the light, and divided the latter by the former to calculate the final-to-peak ratio. Responses that were more sustained resulted in higher final-to-peak ratios. As seen in Fig. 3C (*black columns*), the averaged final-to-peak ratio was almost zero for M1, but somewhat higher for the others.

The intermediate intensity, 11.6±0.2 log photons cm^{-2} s^{-1}, was well above M1's intrinsic photoresponse threshold but evoked small or no intrinsic responses in M2 – M5 cells (Figs. 4B,D, and 5A,C). M1's response first showed a transient depolarization, then a broader one that outlasted the stimulus (Figs. 3A and 3B). As demonstrated previously, the early response is rod/cone-driven while the delayed component is intrinsically generated (Wong et al., 2007a). The delayed response caused M1 cells' final-to-peak amplitude ratio to become much higher than for the lower stimulus intensity (Fig. 3C). Non-M1 cells' responses at the intermediate intensity were also somewhat more sustained than at the lower intensity and so their final-to-peak ratios also became higher (Fig. 3C), but unlike M1 cells, their responses terminated rapidly at light offset (Fig. 3B), presumably due to the near absence of intrinsic responses.

The highest intensity tested, 13.6±0.3 log photons cm^{-2} s^{-1}, was sufficient to evoke robust intrinsic responses in all ipRGC types (Figs. 4A,B,D, and 5A,C), and all cells stayed depolarized for many seconds after lights off (Figs. 3A and 3B).

Intrinsic light responses

To assess intrinsic photosensitivity in isolation, we next recorded light responses in the presence of rod/cone signaling blockers. Fig. 4A shows representative examples, and Fig. 4B shows averaged responses with all spikes filtered out to highlight the underlying graded potential changes. All cells' intrinsic responses were depolarizing at all intensities, required at least one second to peak, and continued for many seconds after stimulus offset. However, several type-dependent differences were observed. Specifically, M1 had shorter latencies to peak, lower intensity thresholds and higher peak amplitudes than all other ipRGCs, whereas M3's responses tended to be the smallest among the five cell types. These differences are quantified in Figs. 4C and 4D. Curiously, at relatively high stimulus intensities, M1 cells' intrinsic photoresponses often had a transient hyperpolarization several seconds after lights on (Fig. 4B), reminiscent of that seen in Berson et al., 2002. The cause of this dip is unknown.

As mentioned earlier, most of our non-M1 ipRGCs lacked melanopsin immunoreactivity, suggesting that they either do not use melanopsin to sense light or contain very low levels of this protein. To probe whether their intrinsic photosensitivity is melanopsin-based, we determined the λ_{max} of the intrinsic light responses of 6 M2 cells, 2 M3 cells, 8 M4 cells and 6 M5 cells. The method for measuring λ_{max} is explained in the Methods section and illustrated in Fig. 4E. Their mean λ_{max} was 477±1 nm, close to melanopsin's λ_{max} of ~480

NIH-PA Author Manuscript

NIH-PA Author Manuscript

NIH-PA Author Manuscript

nm (Bailes and Lucas, 2013; Panda et al., 2005; Qiu et al., 2005), suggesting that M2 – M5 cells probably use this molecule as their photopigment.

In the final set of analyses (Fig. 5), we compared the five ipRGC types' melanopsin-based spiking responses to light. These analyses are beneficial to the field because MEA spike recordings have been used to compare the melanopsin photoresponses of different types of rodent ipRGCs (Karnas et al., 2013; Perez-Leighton et al., 2011; Tu et al., 2006; Tu et al., 2005) but since this method is done "blind", researchers have been unable to assign cell types to their recordings. Establishing the correspondence between MEA- and whole-cell-recorded cell types would help overcome this problem.

We analyzed not only the rat ipRGCs from the present study, but also the mouse ipRGCs we recorded previously (Zhao et al., 2014). The spike histograms in Fig. 5A show the five rat ipRGC types' averaged intrinsic responses to 10-sec light steps at several intensities. Similar to the graded intrinsic responses shown in Fig. 4, all cells' spiking responses were sluggish, taking at least one second to peak and continuing for many seconds after lights off. Also consistent with the graded responses, M1's spiking responses had the shortest latencies to peak and lowest thresholds. As quantified in Fig. 5B, M1 responses peaked the fastest at all light intensities, whereas the other cell types' latencies to peak formed a separate cluster. Although M1 cells had the lowest thresholds, at relatively high intensities, their response amplitudes were only intermediate among ipRGCs, slightly higher than M3 and M5 but much lower than M2 and M4 (Fig. 5C). Thus, in terms of kinetics and amplitude, three varieties of melanopsin-driven spiking responses are apparent in rat: fast but small (M1), slow and small (M3 and M5), and slow but large (M2 and M4).

Figs. 5D – 5F show the averaged spike histograms, latencies to peak and peak amplitudes of mouse ipRGCs' intrinsic light responses. Just like for rat, these mouse responses peaked slowly and persisted for many seconds after lights off, although post-stimulus spiking tended to return to baseline slightly faster (compare Figs. 5A and 5D). The distribution of latencies to peak paralleled that for rat ipRGCs: M1 cells peaked the fastest at all stimulus intensities, whereas the other cell types had comparable latencies (Fig. 5E). Also similar to rat, the M1 cells in mouse had the lowest intensity thresholds (Fig. 5F). But in contrast to rat, the responses of mouse M3 and M5 cells to high light intensities exceeded those of M1 cells, nearly matching those of M2 and M4 (Fig. 5F). In summary, in terms of kinetics and amplitude, mouse ipRGCs exhibit only two obvious varieties of melanopsin-based spiking responses: fast but small (M1), and slow but large (M2 – M5).

4. Discussion

Melanopsin expression in rat ipRGCs

The melanopsin antibody we used was originally reported to stain only OFF-stratifying ipRGCs, now called M1 cells (Hattar et al., 2002). We lengthened the antibody incubation and managed to label some M2 cells, though none of the M3 – M5 cells tested showed staining. Sensitive immunoperoxidase-based methods enabled this antibody to label M3 as well as M1 and M2, strongly suggesting that melanopsin is the photopigment of these types (Esquiva et al., 2013). Though melanopsin expression has not been demonstrated for rat M4

NIH-PA Author Manuscript

NIH-PA Author Manuscript

NIH-PA Author Manuscript

or M5 cells, they likely use this molecule as their photopigment because their intrinsic photoresponses have a λ_{max} close to melanopsin's λ_{max}, and because their counterparts in mouse have been shown through immunohistochemistry (Estevez et al., 2012) and GFP labeling (Ecker et al., 2010) to contain melanopsin. The difficulty in revealing melanopsin immunoreactivity in M4 and M5 (Esquiva et al., 2013) suggests that they have the lowest expression levels among rat ipRGCs. However, their intrinsic photoresponses are about as large as those of M2 and seemingly larger than those of M3 (Fig. 4D), indicating that melanopsin density may not be the only determinant of response amplitude.

Morphological comparison with mouse ipRGCs

The existence of five types of ipRGCs in mouse was first demonstrated by GFP labeling of melanopsin-expressing neurons (Ecker et al., 2010). But genetic labeling of melanopsin-expressing cells is not guaranteed to label all ipRGCs (Do et al., 2009; Schmidt et al., 2008), raising the possibility that the five types labeled by Ecker *et al.* are incomplete. Here, we relied on whole-cell recording instead of genetics to search for ipRGCs in rat. Specifically, we recorded from a large number of RGCs and looked for those generating sustained light responses that persisted during rod/cone signaling block. Five cell types were found, all with morphologies resembling those in mouse, suggesting that they probably account for all rat and mouse ipRGC types. Nonetheless, we cannot rule out additional ipRGCs that generate transient, sub-spiking-threshold intrinsic photoresponses, which would have been discarded in our screen for sustained RGCs, and which would also have been undetectable in previous MEA spike recordings.

Morphologically, rat ipRGCs are strikingly similar to their mouse counterparts. Not only do they have identical stratification patterns, but Sholl analyses of dendritic distribution are also in close agreement (Estevez et al., 2012; Hu et al., 2013; Muller et al., 2010; Schmidt and Kofuji, 2010, 2011). Comparison with three previous morphological characterizations of mouse M1 – M4 cells (Berson et al., 2010; Estevez et al., 2012; Schmidt and Kofuji, 2011) reveals additional similarities in soma size, total dendritic length, total branch points, and the number of primary dendrites. For example, the rank order in soma size is M4 > M2 > M3 > M1 for both species. Furthermore, both mouse and rat M4 cells have greater total dendritic length than M1 – M3 cells. And in both species, M4 cells have more branch points and primary dendrites than M1 and M2 cells (these parameters were not quantified for mouse M3). An additional rat-versus-mouse similarity is that in both cases, M3 seems to resemble M2 more than M1 – as shown in Table 1B, no significant difference was observed between rat M3 and M2 for any of the five parameters. However, whereas mouse M1 cells have smaller dendritic fields than M2 – M4 cells, rat M1 cells' dendritic fields are larger than those of M2 – M5 (Table 1A).

Interestingly, we seem to have encountered M5 cells more frequently in rat than when we recorded from GFP-labeled mouse ipRGCs (Ecker et al., 2010; Hu et al., 2013; Zhao et al., 2014). Since an RGC type is expected to tile the entire retina (Masland, 2001), the rarity of GFP-labeled mouse M5 cells has led to the speculation that it is either not a true cell type, or that only a subset of M5 cells is labeled in this particular GFP line. The relatively high frequency of M5 cells in the present study suggests that M5 may be a true cell type. On the

NIH-PA Author Manuscript

NIH-PA Author Manuscript

NIH-PA Author Manuscript

other hand, just like in our previous mouse studies, we came across very few M3 cells in rat, reinforcing the idea that it is not a true RGC type but is instead an anomalous hybrid of M1 and M2 (Berson et al., 2010).

Physiological comparison with mouse ipRGCs

All previously published whole-cell recordings of rat ipRGCs were made from M1 cells, which were all identified through epifluorescence imaging of dyes retrogradely transported from the SCN (Berson et al., 2002; Graham et al., 2008; Perez-Leon et al., 2006; Van Hook and Berson, 2010; Van Hook et al., 2012; Warren et al., 2003, 2006; Wong et al., 2005; Wong et al., 2007a). Although Estevez et al., 2012 reported intrinsic photoresponses in two rat M4 cells, such responses were not shown. Thus, the whole-cell recordings presented here are the first published recordings of not only rat M2 – M5 cells, but also dark-adapted rat M1 cells.

We recently characterized the resting properties and light responses of all five types of mouse ipRGCs under dark-adapted conditions (Zhao et al., 2014). To some extent, the resting potentials and spontaneous spike rates of rat ipRGCs paralleled those of mouse ipRGCs. In both species, M2 and M4 had somewhat more positive resting potentials than the other types. In addition, M4 spiked in darkness at the highest rate while M1 displayed the least spontaneous spiking, although all cell types spiked at higher rates in mouse than in rat.

Similarity between the two species was also seen for the extrinsic light responses of M2 – M5 cells, in that all of them were tonic. By contrast, whereas mouse M1 cells' extrinsic light responses were as tonic as those of M2 – M5, rat M1 cells responded very transiently. We had previously recorded very transient and small extrinsic photoresponses from epifluorescence-targeted rat M1 cells, and attributed the transience to the light-adapted state of the cells (Wong et al., 2007a). Indeed, the extrinsic photoresponses of epifluorescence-targeted mouse M1 cells were also relatively transient (Schmidt and Kofuji, 2010). But here we found dark-adapted rat M1 cells' extrinsic photoresponses to be similarly transient and small, suggesting that they receive weaker rod input than their mouse counterpart. Since M1 is the predominant RGC type that signals to the circadian clock (Baver et al., 2008; Berson et al., 2002; Ecker et al., 2010), this rat-versus-mouse discrepancy could account for the different photoentrainment thresholds that have been reported for mouse versus other species. Numerous studies have shown that mice can be photoentrained by rod signals channeled by M1 cells to the SCN, enabling entrainment to light/dark cycles as dim as ~ 8 log photons cm^{-2} s^{-1} (Altimus et al., 2010; Butler and Silver, 2011; Ebihara and Tsuji, 1980; Lall et al., 2010; Morin and Studholme, 2011). However, much higher thresholds have been reported for the circadian systems of rat (McGuire et al., 1973), hamster (Hut et al., 2008; Takahashi et al., 1984) and human (Brainard et al., 2001; Thapan et al., 2001; Zeitzer et al., 2000). It seems reasonable to hypothesize that the mouse SCN receives stronger rod input than for the other three species, which might reconcile the ongoing debate about the role of rods in photoentrainment (for examples, see(Lall et al., 2010)and(Gooley et al., 2010). This difference between mouse and other species also suggests that rat may be better than mouse as a model for understanding the human photoentrainment system.

NIH-PA Author Manuscript

NIH-PA Author Manuscript

NIH-PA Author Manuscript

The graded intrinsic photoresponses of mouse and rat ipRGCs were fairly similar. Most notably, M1's responses were the fastest, largest, and lowest-threshold in both species (Zhao et al., 2014). While all ipRGCs' action potentials became smaller during their intrinsic light responses, such reduction was especially pronounced for rat M1 cells, which exhibited virtually complete depolarization block at high stimulus intensities (Fig. 4A). While this is partly due to M1 cells' unusually large intrinsic photoresponses, we have also found them to be more likely than the other ipRGCs to cease spiking upon current-induced depolarization (Hu et al., 2013). Despite depolarization block during high-intensity photostimulation, rat M1 cells can still signal to the circadian system because intense light presented to the retinas evoked robust responses in postsynaptic SCN neurons (Wong et al., 2007b).

MEA recording is used increasingly to measure ipRGC photoresponses because it is technically easy, has a high throughput, and does not require cell-specific fluorescent labeling. But since MEA recording is done without knowledge of cellular morphology, researchers have been unable to assign cell types to their recordings, which motivated us to analyze the spiking intrinsic photoresponses of whole-cell-recorded rat and mouse ipRGCs. In rat, M2 and M4 responses were so similar that we do not believe they can be reliably distinguished on an MEA. While M2 and M4 do have different spike widths (Hu et al., 2013), the difference is probably too subtle for telling them apart. The responses of M1 and M5 reached saturation at comparable amplitudes (~20 Hz), though the former's faster kinetics and lower thresholds should allow it to be distinguished from the latter. M3 cells appeared to respond with lower amplitudes than all the other cell types and so it might be possible to identify them on an MEA, although this would not be easy considering that M3 and M5 had virtually identical kinetics and thresholds. Thus, we recommend classifying MEA-recorded rat ipRGCs into three groups, based on the kinetics and amplitudes of their intrinsic photoresponses: fast but small (M1), slow and small (M3 and M5), and slow but large (M2 and M4). On the other hand, for mouse ipRGCs, M3 and M5 were less distinguishable from M2 and M4 (compare Figs. 5C and 5F), and so we suggest classifying MEA recordings of mouse ipRGCs into just two groups: M1 (with fast, low-threshold responses), and non-M1 (with slow, high-threshold responses). An important caveat is that the light responses presented here may not be quantitatively identical to MEA-recorded responses, because the physiology of whole-cell-recorded cells could be altered by dialysis of intracellular ions and of diffusible cytosolic constituents. Nevertheless, we do find all three varieties of rat ipRGC photoresponses in our MEA recordings (O. Walch, L. Zhang, D. Forger and K. Wong, manuscript in preparation), and Van Gelder and colleagues' MEA recordings of adult mouse retinas have indeed revealed only two types of melanopsin photoresponses (Tu et al., 2005).

Do other mammalian species also have multiple types of ipRGCs?

Besides rat and mouse, melanopsin expression has been examined in at least eleven other mammalian species. Melanopsin-positive RGC somas were observed in cat (Semo et al., 2005), fat-tailed dunnart (Pires et al., 2007) and guinea pig (Wang et al., 2011), but dendritic morphologies were not analyzed and so it remains unknown whether these species have multiple ipRGC types. In hamster, melanopsin antibody staining was seen nearly exclusively in the OFF sublamina of the IPL (Sollars et al., 2003), consistent with M1 being the only

NIH-PA Author Manuscript

NIH-PA Author Manuscript

NIH-PA Author Manuscript

type present. Reinforcing this possibility, melanopsin-immunopositive cells in hamster have been shown to project mainly to the SCN, intergeniculate leaflet, ventral lateral geniculate nucleus (LGN) and olivary pretectal nucleus (Morin et al., 2003), which are known to be the primary central targets of M1 cells in mouse (Ecker et al., 2010; Hattar et al., 2006). On the other hand, Morin *et al.* also observed modest projection of these cells to the dorsal LGN, which in mouse receives input only from non-M1 ipRGCs (Brown et al., 2010; Ecker et al., 2010), implicating the existence of non-M1 cells in hamster.

Melanopsin-positive cells with M1- and M2-like morphologies were detected in Sudanian grass rat, and MEA recordings from neonatal retinas showed three varieties of melanopsin-based photoresponses, suggesting this species might have three or more ipRGC types (Karnas et al., 2013). In rabbit, melanopsin immunohistochemistry revealed not only M1 and M2 cells, but also bistratifying cells that were presumably M3 cells (Hoshi et al., 2009). In squirrel, all melanopsin antibodies attempted have failed to stain any RGCs (Wei Li, personal communication), but western blots using these antibodies do reveal melanopsin expression, and ON alpha RGCs are intrinsically photosensitive (Schmidt et al., 2014). Thus, squirrel definitely has M4 cells, though the lack of melanopsin immunostaining points to the absence of M1 or M2. In a paper examining gerbil RGCs innervating the dorsal raphe nucleus, a melanopsin-positive RGC is shown and it appears to be bistratified, suggesting it was M3 (Luan et al., 2011). Interestingly, Luan *et al.* found that rod/cone blockade abolished all ON alpha RGCs' photoresponses, indicating that intrinsic photosensitivity is not common to all ON alpha cells.

Two morphological types of melanopsin-positive cells have been reported in three primate species: marmoset (Jusuf et al., 2007), macaque and human (Dacey et al., 2005). Both types have sparse dendrites and monostratify in either the ON or OFF sublamina. Thus, they resemble the M1 and M2 cells of rodents, and have been referred to as such (Neumann et al., 2011). However, these primate RGCs are not functionally equivalent to the M1 and M2 cells. First, the M1-like cells project to the dLGN (Dacey et al., 2005), but as mentioned earlier, mouse M1 cells do not. Second, the M2-like cells do not possess center/surround antagonism in their receptive fields (Dacey et al., 2005), whereas mouse M2 cells do (Zhao et al., 2014). In macaque, the vast majority of melanopsin-immunopositive RGCs also contain pituitary adenylate cyclase-activating polypeptide (PACAP), a neuropeptide present in SCN-projecting RGCs (Hannibal et al., 2014). However, an occasional PACAP-immunopositive RGC was found to lack melanopsin immunostaining (Hannibal et al., 2014), and so additional ipRGC types with very low melanopsin levels could exist in primates.

In conclusion, having multiple types of ipRGCs may be a common theme across mammalian species. As discussed above, without amplification, melanopsin antibodies tend to stain only the ipRGC type(s) with the highest expression levels. Thus, it is possible that these species have more types of ipRGCs than suggested by the referenced papers.

Acknowledgments

This work was funded by National Eye Institute (NEI) grants R00 EY018863 and R01 EY023660 to K.Y.W., a Research to Prevent Blindness Scientific Career Development Award to K.Y.W., a Health Sciences Scholars

Program Summer Research Stipend to B.Y.L., and NEI Vision Core Grant P30 EY007003 to the Kellogg Eye Center.

Abbreviations

ChAT	choline acetyltransferase
D-AP5	D-2-amino-5-phosphonovalerate
DNQX	6,7-dinitroquinoxaline2,3-dione
GCL	ganglion cell layer
GFP	green fluorescent protein
IPL	inner plexiform layer
ipRGC	intrinsically photosensitive retinal ganglion cell
L-AP4	L(+)-2-amino-4-phosphonobutyrate
LGN	lateral geniculate nucleus
MEA	multielectrode array
ND	neutral density
PACAP	pituitary adenylate cyclase-activating polypeptide
PBS	phosphate buffer saline
RBPMS	RNA-binding protein with multiple splicing
RGC	retinal ganglion cell
SCN	suprachiasmatic nucleus

References

Altimus CM, Guler AD, Alam NM, Arman AC, Prusky GT, Sampath AP, Hattar S. Rod photoreceptors drive circadian photoentrainment across a wide range of light intensities. Nat Neurosci. 2010; 13:1107–1112. [PubMed: 20711184]

Bailes HJ, Lucas RJ. Human melanopsin forms a pigment maximally sensitive to blue light (lambdamax approximately 479 nm) supporting activation of G(q/11) and G(i/o) signalling cascades. Proc Biol Sci. 2013; 280:20122987. [PubMed: 23554393]

Baver SB, Pickard GE, Sollars PJ. Two types of melanopsin retinal ganglion cell differentially innervate the hypothalamic suprachiasmatic nucleus and the olivary pretectal nucleus. Eur J Neurosci. 2008; 27:1763–1770. [PubMed: 18371076]

Berson DM, Castrucci AM, Provencio I. Morphology and mosaics of melanopsin-expressing retinal ganglion cell types in mice. J Comp Neurol. 2010; 518:2405–2422. [PubMed: 20503419]

Berson DM, Dunn FA, Takao M. Phototransduction by retinal ganglion cells that set the circadian clock. Science. 2002; 295:1070–1073. [PubMed: 11834835]

Boudard DL, Mendoza J, Hicks D. Loss of photic entrainment at low illuminances in rats with acute photoreceptor degeneration. Eur J Neurosci. 2009; 30:1527–1536. [PubMed: 19821841]

Brainard GC, Hanifin JP, Greeson JM, Byrne B, Glickman G, Gerner E, Rollag MD. Action spectrum for melatonin regulation in humans: evidence for a novel circadian photoreceptor. J Neurosci. 2001; 21:6405–6412. [PubMed: 11487664]

NIH-PA Author Manuscript NIH-PA Author Manuscript NIH-PA Author Manuscript

NIH-PA Author Manuscript NIH-PA Author Manuscript NIH-PA Author Manuscript

Brown TM, Gias C, Hatori M, Keding SR, Semo M, Coffey PJ, Gigg J, Piggins HD, Panda S, Lucas RJ. Melanopsin contributions to irradiance coding in the thalamo-cortical visual system. PLoS Biol. 2010; 8:e1000558. [PubMed: 21151887]

Butler MP, Silver R. Divergent photic thresholds in the non-image-forming visual system: entrainment, masking and pupillary light reflex. Proc Biol Sci. 2011; 278:745–750. [PubMed: 20861055]

Dacey DM, Liao HW, Peterson BB, Robinson FR, Smith VC, Pokorny J, Yau KW, Gamlin PD. Melanopsin-expressing ganglion cells in primate retina signal colour and irradiance and project to the LGN. Nature. 2005; 433:749–754. [PubMed: 15716953]

Do MT, Kang SH, Xue T, Zhong H, Liao HW, Bergles DE, Yau KW. Photon capture and signalling by melanopsin retinal ganglion cells. Nature. 2009; 457:281–287. [PubMed: 19118382]

Ebihara S, Tsuji K. Entrainment of the circadian activity rhythm to the light cycle: effective light intensity for a Zeitgeber in the retinal degenerate C3H mouse and the normal C57BL mouse. Physiol Behav. 1980; 24:523–527. [PubMed: 7375573]

Ecker JL, Dumitrescu ON, Wong KY, Alam NM, Chen SK, LeGates T, Renna JM, Prusky GT, Berson DM, Hattar S. Melanopsin-expressing retinal ganglion-cell photoreceptors: cellular diversity and role in pattern vision. Neuron. 2010; 67:49–60. [PubMed: 20624591]

Engelund A, Fahrenkrug J, Harrison A, Hannibal J. Vesicular glutamate transporter 2 (VGLUT2) is co-stored with PACAP in projections from the rat melanopsin-containing retinal ganglion cells. Cell Tissue Res. 2010; 340:243–255. [PubMed: 20339872]

Esquiva G, Lax P, Cuenca N. Impairment of intrinsically photosensitive retinal ganglion cells associated with late stages of retinal degeneration. Invest Ophthalmol Vis Sci. 2013; 54:4605–4618. [PubMed: 23766478]

Estevez ME, Fogerson PM, Ilardi MC, Borghuis BG, Chan E, Weng S, Auferkorte ON, Demb JB, Berson DM. Form and function of the M4 cell, an intrinsically photosensitive retinal ganglion cell type contributing to geniculocortical vision. J Neurosci. 2012; 32:13608–13620. [PubMed: 23015450]

Gooley JJ, Rajaratnam SM, Brainard GC, Kronauer RE, Czeisler CA, Lockley SW. Spectral responses of the human circadian system depend on the irradiance and duration of exposure to light. Sci Transl Med. 2010; 2:31ra33.

Graham DM, Wong KY, Shapiro P, Frederick C, Pattabiraman K, Berson DM. Melanopsin ganglion cells use a membrane-associated rhabdomeric phototransduction cascade. J Neurophysiol. 2008; 99:2522–2532. [PubMed: 18305089]

Hannibal J, Georg B, Fahrenkrug J. Differential expression of melanopsin mRNA and protein in Brown Norwegian rats. Exp Eye Res. 2013; 106:55–63. [PubMed: 23187103]

Hannibal J, Kankipati L, Strang CE, Peterson BB, Dacey D, Gamlin PD. Central projections of intrinsically photosensitive retinal ganglion cells in the macaque monkey. J Comp Neurol. 2014; 522:2231–2248. [PubMed: 24752373]

Hattar S, Kumar M, Park A, Tong P, Tung J, Yau KW, Berson DM. Central projections of melanopsin-expressing retinal ganglion cells in the mouse. J Comp Neurol. 2006; 497:326–349. [PubMed: 16736474]

Hattar S, Liao HW, Takao M, Berson DM, Yau KW. Melanopsin-containing retinal ganglion cells: architecture, projections, and intrinsic photosensitivity. Science. 2002; 295:1065–1070. [PubMed: 11834834]

Hoshi H, Liu WL, Massey SC, Mills SL. ON inputs to the OFF layer: bipolar cells that break the stratification rules of the retina. J Neurosci. 2009; 29:8875–8883. [PubMed: 19605625]

Hu C, Hill DD, Wong KY. Intrinsic physiological properties of the five types of mouse ganglion-cell photoreceptors. J Neurophysiol. 2013; 109:1876–1889. [PubMed: 23343892]

Hut RA, Oklejewicz M, Rieux C, Cooper HM. Photic sensitivity ranges of hamster pupillary and circadian phase responses do not overlap. J Biol Rhythms. 2008; 23:37–48. [PubMed: 18258756]

Ingham ES, Gunhan E, Fuller PM, Fuller CA. Immunotoxin-induced ablation of melanopsin retinal ganglion cells in a non-murine mammalian model. J Comp Neurol. 2009; 516:125–140. [PubMed: 19575450]

NIH-PA Author Manuscript NIH-PA Author Manuscript NIH-PA Author Manuscript

Jusuf PR, Lee SC, Hannibal J, Grunert U. Characterization and synaptic connectivity of melanopsin-containing ganglion cells in the primate retina. Eur J Neurosci. 2007; 26:2906–2921. [PubMed: 18001286]

Karnas D, Hicks D, Mordel J, Pevet P, Meissl H. Intrinsic photosensitive retinal ganglion cells in the diurnal rodent, Arvicanthis ansorgei. PLoS One. 2013; 8:e73343. [PubMed: 23951350]

Lall GS, Revell VL, Momiji H, Al Enezi J, Altimus CM, Guler AD, Aguilar C, Cameron MA, Allender S, Hankins MW, Lucas RJ. Distinct contributions of rod, cone, and melanopsin photoreceptors to encoding irradiance. Neuron. 2010; 66:417–428. [PubMed: 20471354]

Lamb TD. Photoreceptor spectral sensitivities: common shape in the long-wavelength region. Vision Res. 1995; 35:3083–3091. [PubMed: 8533344]

Li RS, Chen BY, Tay DK, Chan HH, Pu ML, So KF. Melanopsin-expressing retinal ganglion cells are more injury-resistant in a chronic ocular hypertension model. Invest Ophthalmol Vis Sci. 2006; 47:2951–2958. [PubMed: 16799038]

Luan L, Ren C, Lau BW, Yang J, Pickard GE, So KF, Pu M. Y-like retinal ganglion cells innervate the dorsal raphe nucleus in the Mongolian gerbil (Meriones unguiculatus). PLoS One. 2011; 6:e18938. [PubMed: 21552551]

Masland RH. The fundamental plan of the retina. Nat Neurosci. 2001; 4:877–886. [PubMed: 11528418]

McGuire RA, Rand WM, Wurtman RJ. Entrainment of the body temperature rhythm in rats: effect of color and intensity of environmental light. Science. 1973; 181:956–957. [PubMed: 4730449]

Morin LP, Blanchard JH, Provencio I. Retinal ganglion cell projections to the hamster suprachiasmatic nucleus, intergeniculate leaflet, and visual midbrain: bifurcation and melanopsin immunoreactivity. J Comp Neurol. 2003; 465:401–416. [PubMed: 12966564]

Morin LP, Studholme KM. Separation of function for classical and ganglion cell photoreceptors with respect to circadian rhythm entrainment and induction of photosomnolence. Neuroscience. 2011; 199:213–224. [PubMed: 21985934]

Muller LP, Do MT, Yau KW, He S, Baldridge WH. Tracer coupling of intrinsically photosensitive retinal ganglion cells to amacrine cells in the mouse retina. J Comp Neurol. 2010; 518:4813–4824. [PubMed: 20963830]

Neumann S, Haverkamp S, Auferkorte ON. Intrinsically photosensitive ganglion cells of the primate retina express distinct combinations of inhibitory neurotransmitter receptors. Neuroscience. 2011; 199:24–31. [PubMed: 22044923]

Ostergaard J, Hannibal J, Fahrenkrug J. Synaptic contact between melanopsin-containing retinal ganglion cells and rod bipolar cells. Invest Ophthalmol Vis Sci. 2007; 48:3812–3820. [PubMed: 17652756]

Panda S, Nayak SK, Campo B, Walker JR, Hogenesch JB, Jegla T. Illumination of the melanopsin signaling pathway. Science. 2005; 307:600–604. [PubMed: 15681390]

Perez-Leighton CE, Schmidt TM, Abramowitz J, Birnbaumer L, Kofuji P. Intrinsic phototransduction persists in melanopsin-expressing ganglion cells lacking diacylglycerol-sensitive TRPC subunits. Eur J Neurosci. 2011; 33:856–867. [PubMed: 21261756]

Perez-Leon JA, Warren EJ, Allen CN, Robinson DW, Brown RL. Synaptic inputs to retinal ganglion cells that set the circadian clock. Eur J Neurosci. 2006; 24:1117–1123. [PubMed: 16930437]

Pires SS, Shand J, Bellingham J, Arrese C, Turton M, Peirson S, Foster RG, Halford S. Isolation and characterization of melanopsin (Opn4) from the Australian marsupial Sminthopsis crassicaudata (fat-tailed dunnart). Proc Biol Sci. 2007; 274:2791–2799. [PubMed: 17785267]

Provencio I, Jiang G, De Grip WJ, Hayes WP, Rollag MD. Melanopsin: An opsin in melanophores, brain, and eye. Proc Natl Acad Sci U S A. 1998; 95:340–345. [PubMed: 9419377]

Qiu X, Kumbalasiri T, Carlson SM, Wong KY, Krishna V, Provencio I, Berson DM. Induction of photosensitivity by heterologous expression of melanopsin. Nature. 2005; 433:745–749. [PubMed: 15674243]

Rodriguez AR, de Sevilla Muller LP, Brecha NC. The RNA binding protein RBPMS is a selective marker of ganglion cells in the mammalian retina. J Comp Neurol. 2014; 522:1411–1443. [PubMed: 24318667]

NIH-PA Author Manuscript NIH-PA Author Manuscript NIH-PA Author Manuscript

Schmidt TM, Alam NM, Chen S, Kofuji P, Li W, Prusky GT, Hattar S. A role for melanopsin in alpha retinal ganglion cells and contrast detection. Neuron. 2014; 82:781–788. [PubMed: 24853938]

Schmidt TM, Kofuji P. Differential cone pathway influence on intrinsically photosensitive retinal ganglion cell subtypes. J Neurosci. 2010; 30:16262–16271. [PubMed: 21123572]

Schmidt TM, Kofuji P. Structure and function of bistratified intrinsically photosensitive retinal ganglion cells in the mouse. J Comp Neurol. 2011; 519:1492–1504. [PubMed: 21452206]

Schmidt TM, Taniguchi K, Kofuji P. Intrinsic and extrinsic light responses in melanopsin-expressing ganglion cells during mouse development. J Neurophysiol. 2008; 100:371–384. [PubMed: 18480363]

Semo M, Munoz Llamosas M, Foster RG, Jeffery G. Melanopsin (Opn4) positive cells in the cat retina are randomly distributed across the ganglion cell layer. Vis Neurosci. 2005; 22:111–116. [PubMed: 15842746]

Sholl DA. Dendritic organization in the neurons of the visual and motor cortices of the cat. J Anat. 1953; 87:387–406. [PubMed: 13117757]

Sodhi P, Hartwick AT. Adenosine modulates light responses of rat retinal ganglion cell photoreceptors through cyclic AMP-mediated pathway. J Physiol. 2014

Sollars PJ, Smeraski CA, Kaufman JD, Ogilvie MD, Provencio I, Pickard GE. Melanopsin and non-melanopsin expressing retinal ganglion cells innervate the hypothalamic suprachiasmatic nucleus. Vis Neurosci. 2003; 20:601–610. [PubMed: 15088713]

Takahashi JS, DeCoursey PJ, Bauman L, Menaker M. Spectral sensitivity of a novel photoreceptive system mediating entrainment of mammalian circadian rhythms. Nature. 1984; 308:186–188. [PubMed: 6700721]

Thapan K, Arendt J, Skene DJ. An action spectrum for melatonin suppression: evidence for a novel non-rod, non-cone photoreceptor system in humans. J Physiol. 2001; 535:261–267. [PubMed: 11507175]

Tu DC, Owens LA, Anderson L, Golczak M, Doyle SE, McCall M, Menaker M, Palczewski K, Van Gelder RN. Inner retinal photoreception independent of the visual retinoid cycle. Proc Natl Acad Sci U S A. 2006; 103:10426–10431. [PubMed: 16788071]

Tu DC, Zhang D, Demas J, Slutsky EB, Provencio I, Holy TE, Van Gelder RN. Physiologic diversity and development of intrinsically photosensitive retinal ganglion cells. Neuron. 2005; 48:987–999. [PubMed: 16364902]

Van Hook MJ, Berson DM. Hyperpolarization-activated current (I(h)) in ganglion-cell photoreceptors. PLoS One. 2010; 5:e15344. [PubMed: 21187958]

Van Hook MJ, Wong KY, Berson DM. Dopaminergic modulation of ganglion-cell photoreceptors in rat. Eur J Neurosci. 2012; 35:507–518. [PubMed: 22304466]

Viney TJ, Balint K, Hillier D, Siegert S, Boldogkoi Z, Enquist LW, Meister M, Cepko CL, Roska B. Local retinal circuits of melanopsin-containing ganglion cells identified by transsynaptic viral tracing. Curr Biol. 2007; 17:981–988. [PubMed: 17524644]

Wang F, Zhou J, Lu Y, Chu R. Effects of 530 nm green light on refractive status, melatonin, MT1 receptor, and melanopsin in the guinea pig. Curr Eye Res. 2011; 36:103–111. [PubMed: 21158589]

Warren EJ, Allen CN, Brown RL, Robinson DW. Intrinsic light responses of retinal ganglion cells projecting to the circadian system. Eur J Neurosci. 2003; 17:1727–1735. [PubMed: 12752771]

Warren EJ, Allen CN, Brown RL, Robinson DW. The light-activated signaling pathway in SCN-projecting rat retinal ganglion cells. Eur J Neurosci. 2006; 23:2477–2487. [PubMed: 16706854]

Weng S, Wong KY, Berson DM. Circadian modulation of melanopsin-driven light response in rat ganglion-cell photoreceptors. J Biol Rhythms. 2009; 24:391–402. [PubMed: 19755584]

Wong KY. A retinal ganglion cell that can signal irradiance continuously for 10 hours. J Neurosci. 2012; 32:11478–11485. [PubMed: 22895730]

Wong KY, Dunn FA, Berson DM. Photoreceptor adaptation in intrinsically photosensitive retinal ganglion cells. Neuron. 2005; 48:1001–1010. [PubMed: 16364903]

Wong KY, Dunn FA, Graham DM, Berson DM. Synaptic influences on rat ganglion-cell photoreceptors. J Physiol. 2007a; 582:279–296. [PubMed: 17510182]

NIH-PA Author Manuscript

NIH-PA Author Manuscript

NIH-PA Author Manuscript

Wong KY, Graham DM, Berson DM. The retina-attached SCN slice preparation: an in vitro mammalian circadian visual system. J Biol Rhythms. 2007b; 22:400–410. [PubMed: 17876061]

Zeitzer JM, Dijk DJ, Kronauer R, Brown E, Czeisler C. Sensitivity of the human circadian pacemaker to nocturnal light: melatonin phase resetting and suppression. J Physiol. 2000; 526(Pt 3):695–702. [PubMed: 10922269]

Zhao X, Stafford BK, Godin AL, King WM, Wong KY. Photoresponse diversity among the five types of intrinsically photosensitive retinal ganglion cells. J Physiol. 2014; 592:1619–1636. [PubMed: 24396062]

NIH-PA Author Manuscript

NIH-PA Author Manuscript

NIH-PA Author Manuscript

Highlights

- Ganglion-cell photoreceptors mediate pupil reflexes and circadian photoentrainment.
- Five types of ganglion-cell photoreceptors were recently discovered in mouse.
- We found all five types in rat and analyzed their morphology and electrophysiology.
- All rat ganglion-cell photoreceptors likely use melanopsin as their photopigment.
- Their photoresponses are similar but not identical to those of the mouse cells.

NIH-PA Author Manuscript
NIH-PA Author Manuscript
NIH-PA Author Manuscript

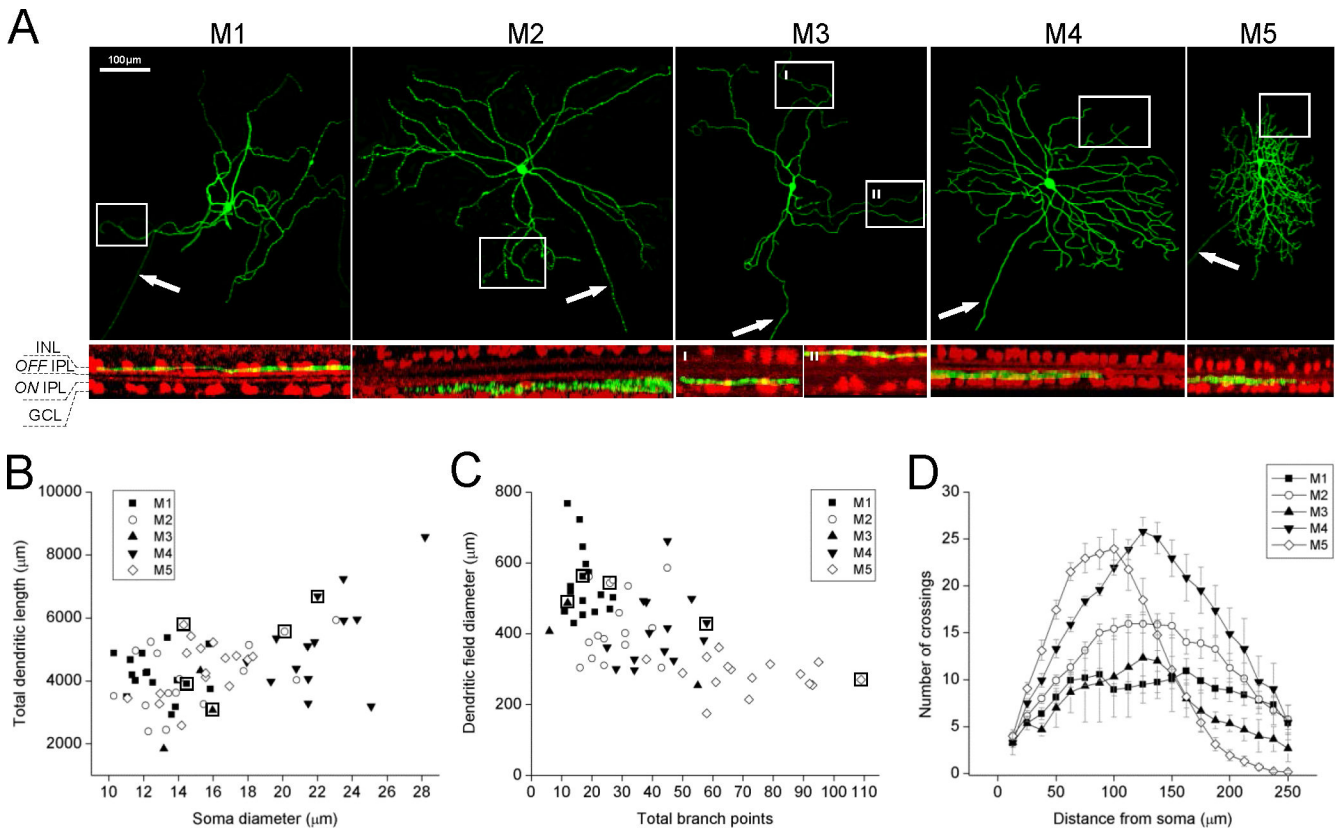

Figure 1. Morphologies of rat ipRGCs

A) *Top row:* Representative z-projected confocal images showing intracellular dye fills of the five ipRGC types. Arrows indicate axons. *Bottom row:* Rotated views of the regions outlined by rectangles in the above z-projections, showing the stratification patterns of distal dendrites. The ChAT bands (*red*) serve as markers for the S2 and S4 sublayers of the inner plexiform layer, which are in the OFF and ON sublaminas respectively. INL, inner nuclear layer; IPL, inner plexiform layer; GCL, ganglion cell layer. *B,C*) Plots of the total dendritic lengths, soma diameters, dendritic-field diameters and total branch points of all ipRGCs analyzed. The data points surrounded by squares correspond to the cells illustrated in panel *A. D*) Sholl analysis of dendritic branching patterns. Concentric circles were drawn at different distances from each cell's soma center, and the number of dendrites crossing each circle was counted. The error bars represent S.E.M. *N* values: M1, 16; M2, 16; M3, 3; M4, 14; M5, 16.

NIH-PA Author Manuscript

NIH-PA Author Manuscript

NIH-PA Author Manuscript

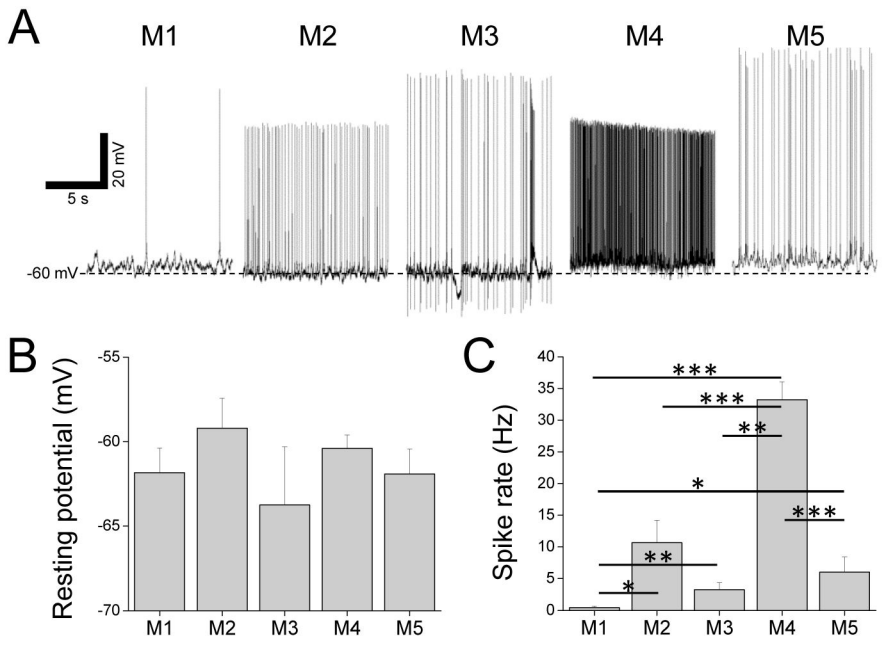

Figure 2. Resting potentials and spontaneous spike rates

A) Examples of current-clamp recordings made from the five ipRGC types in darkness. *B*) Averaged resting membrane potentials. *C*) Averaged spontaneous spike rates. Asterisks indicate significantly different comparisons. *N* values for *B* and *C*: M1, 15; M2, 14; M3, 4; M4, 37; M5, 11.

NIH-PA Author Manuscript
NIH-PA Author Manuscript
NIH-PA Author Manuscript

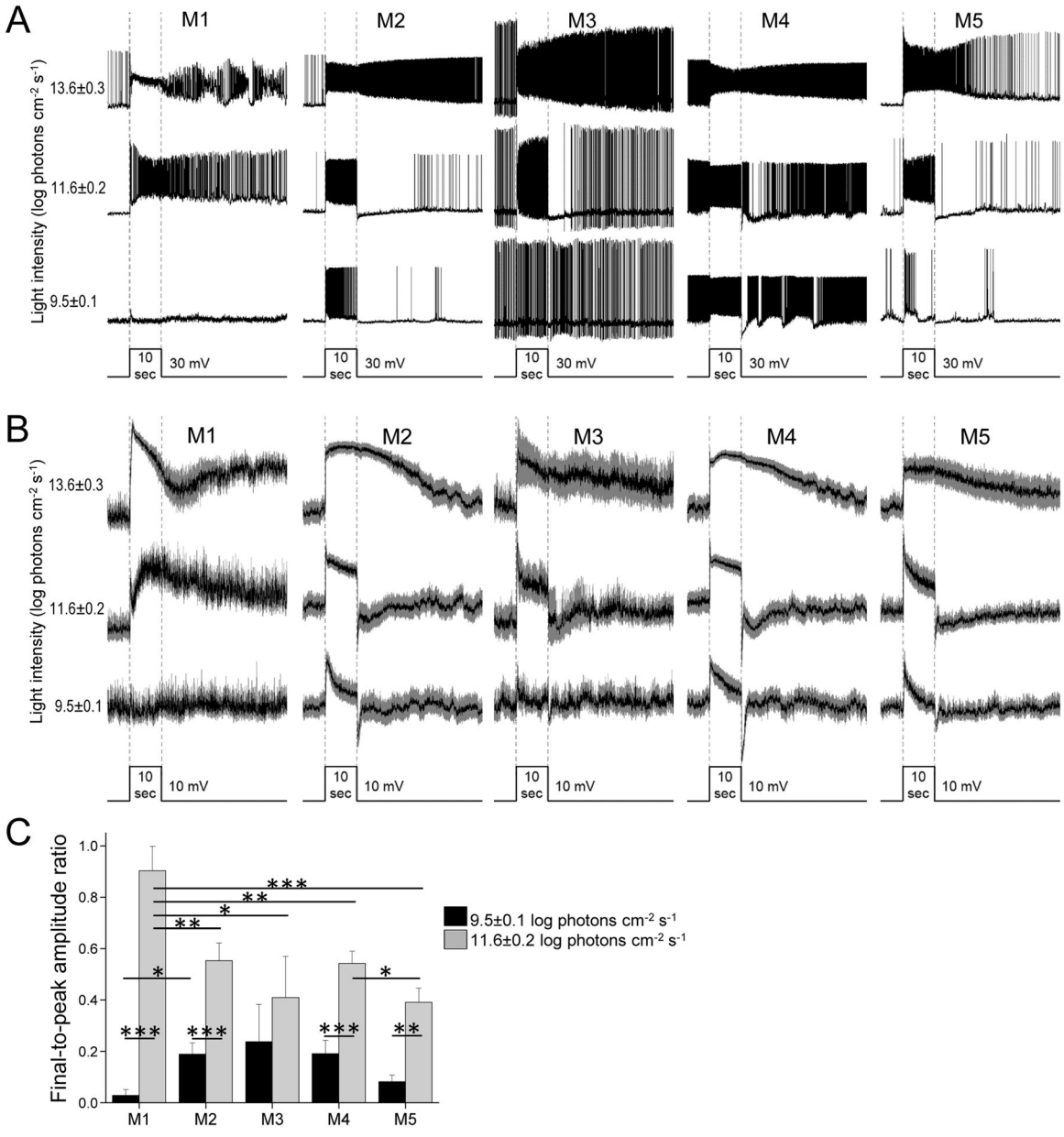

Figure 3. Light responses recorded in normal Ames' medium

A) Example light responses of the five ipRGC types, evoked by 10-sec light steps at three intensities. In the bottom trace, the width of the step indicates stimulus timing and the height of the step serves as a scale bar for response amplitude. *B*) Averaged light responses, with S.E.M. represented by the gray areas. *N* values: M1, 6; M2, 12; M3, 4; M4, 13; M5, 10. *C*) To quantify the kinetics of photoresponse decay, each cell's response amplitude was measured at the peak and near the end of the 10-sec light, and the final-to-peak amplitude ratio was calculated. *Black columns*: Final-to-peak ratios for the responses to the 9.5 log photons cm^{-2} s^{-1} light. *Gray columns*: Final-to-peak ratios for the responses to the 11.6 log photons cm^{-2} s^{-1} light. *N* values were the same as for panel *B*.

NIH-PA Author Manuscript
NIH-PA Author Manuscript
NIH-PA Author Manuscript

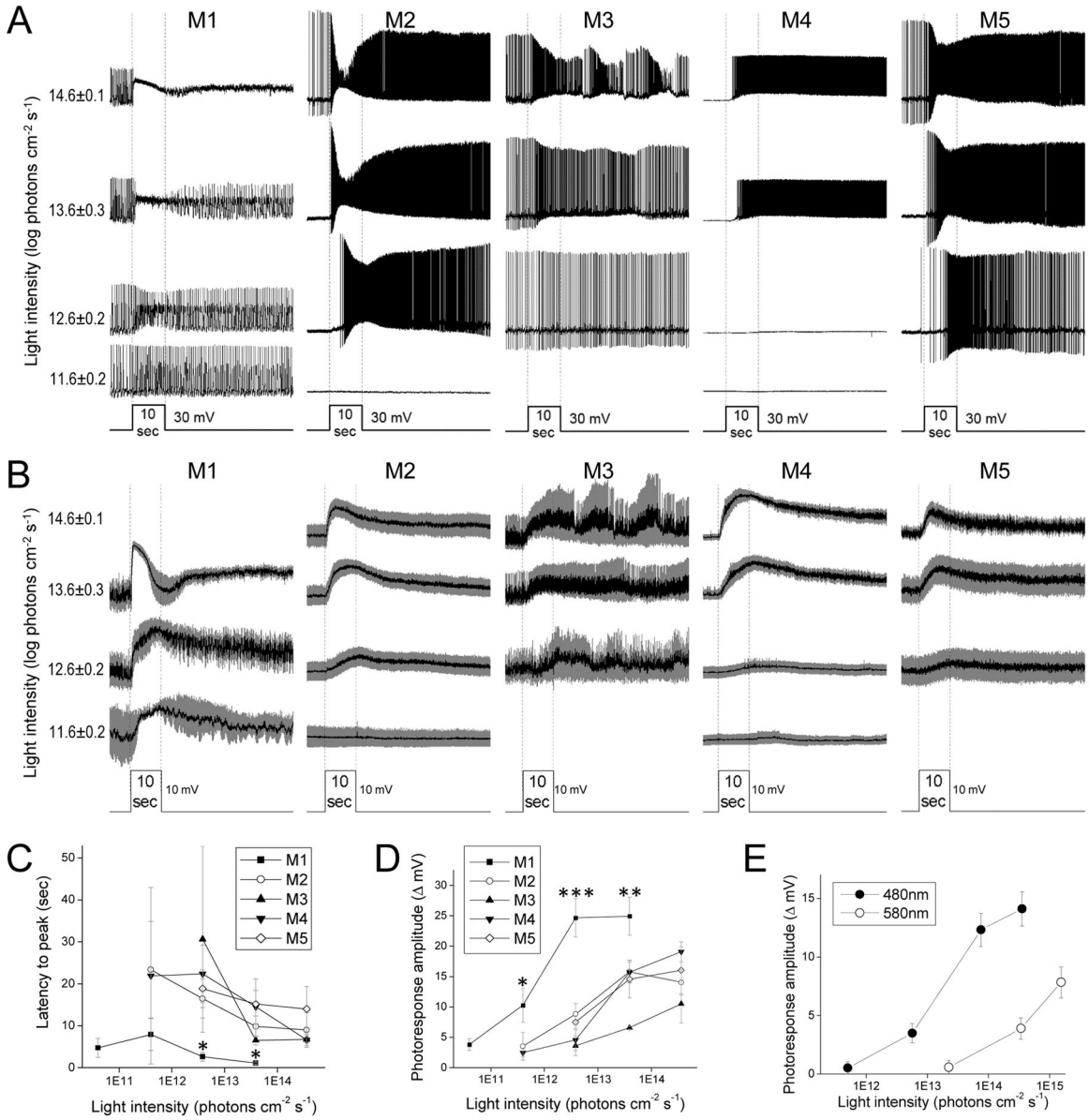

Figure 4. Intrinsic, melanopsin-mediated light responses

A) Example intrinsic photoresponses of the five ipRGC types, evoked by 10-sec light steps. *B*) Averaged intrinsic light responses, with S.E.M. shown in gray. *N* values: M1, 3 – 6; M2, 3 – 9; M3, 2 – 3; M4, 3 – 7; M5, 8 – 10. *C*) Averaged latencies to peak. *D*) Averaged peak response amplitudes. The asterisks mark the M1 data that were significantly different from the other cell types' data. *E*) To determine the λ_{max} of the intrinsic light responses of M2 – M5 cells, their responses to 480 nm and 580 nm lights at several non-saturating intensities were measured. Shown are the averaged response amplitudes. λ_{max} was calculated as described in Methods. *N* values: M2, 6; M3, 2; M4, 8; M5, 6.

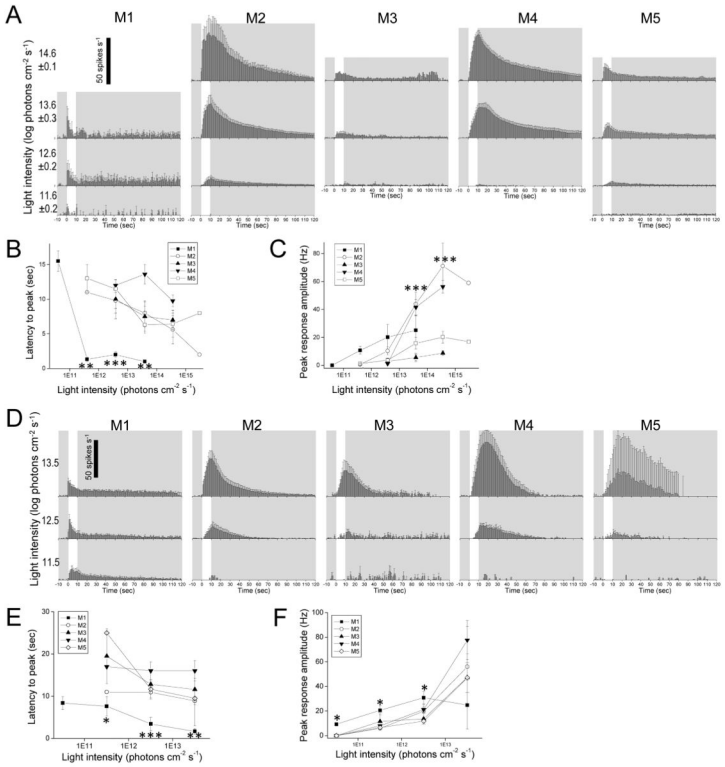

Figure 5. Melanopsin-driven spiking responses to light

The intrinsic photoresponses of rat ipRGCs (*A* – *C*) are compared with those of mouse ipRGCs from Zhao *et al.* 2014 (*D* – *F*). *A*,*D*) Averaged spike histograms with 1-sec bin width. All stimuli were 10-sec light steps that started at time = 0, and are represented by the white regions. *B*,*E*) Averaged latencies to peak. The asterisks highlight the M1 data that were significantly different from those of the other cells. *C*,*F*) Averaged peak amplitudes. In *C*, M2 and M4 were significantly different from the other cell types at the asterisked light intensities. In *F*, M1 was significantly different from the other cells at the asterisked intensities. *N* values for the rat data: M1, 2 – 4; M2, 3 – 7; M3, 1 – 3; M4, 8 – 12; M5, 2 – 8. *N* values for the mouse data: M1, 4 – 10; M2, 10 – 14; M3, 5 – 7; M4, 4 – 9; M5, 2 – 4.

NIH-PA Author Manuscript NIH-PA Author Manuscript NIH-PA Author Manuscript

NIH-PA Author Manuscript NIH-PA Author Manuscript NIH-PA Author Manuscript

Table 1

Group data on morphological measurements

A) Values are mean ± S.E.M. *B*) Statistical comparisons between all possible cell type pairs.

A

	M1 (*n*=16)	M2 (*n*=16)	M3 (*n*=3)	M4 (*n*=14)	M5 (*n*=16)
Soma diameter (μm)	12.8 ± 0.4	15.1 ± 0.9	14.8 ± 0.8	22.2 ± 0.7	15.3 ± 0.5
Dendritic-field diameter (μm)	543.3 ± 24.4	426.4 ± 24.8	382.2 ± 68.1	409.7 ± 26.7	284.8 ± 11.6
Total dendritic length (μm)	4183.6 ± 171.4	4138.5 ± 267.1	3080.8 ± 717.8	5256.1 ± 407.9	4405.5 ± 216.6
Total branch points	17.6 ± 1.2	28.0 ± 2.2	24.3 ± 15.4	41.7 ± 2.7	72.5 ± 4.8
No. of primary dendrites	2.4 ± 0.2	4.2 ± 0.3	3.7 ± 0.7	4.7 ± 0.2	4.4 ± 0.2

B

Soma diameter					Dendritic-field diameter					Total dendritic length					Total branch points					No. of primary dendrites				
	M2	**M3**	**M4**	**M5**		**M2**	**M3**	**M4**	**M5**		**M2**	**M3**	**M4**	**M5**		**M2**	**M3**	**M4**	**M5**		**M2**	**M3**	**M4**	**M5**
M1	*	n.s.	***	***	M1	**	*	***	***	M1	n.s.	*	*	n.s.	M1	***	n.s.	***	***	M1	***	*	***	*
M2		n.s.	***	n.s.	M2		n.s.	n.s.	***	M2		n.s.	*	n.s.	M2		n.s.	***	***	M2		n.s.	n.s.	n.s.
M3			***	n.s.	M3			n.s.	*	M3			*	*	M3			n.s.	**	M3			n.s.	n.s.
M4				***	M4				***	M4				n.s.	M4				***	M4				n.s.

* $p < 0.05$;

** $p < 0.01$;

*** $p < 0.001$;

n.s., no significant difference.